

Microscopic mechanism of plasmon-mediated photocatalytic H_2 splitting on Ag-Au alloy chain

Yuhui Song(宋玉慧), Yirui Lu(芦一瑞), Axin Guo(郭阿鑫), Yifei Cao(曹逸飞), Jinping Li(李金萍), Zhengkun Fu(付正坤), Lei Yan(严蕾), and Zhenglong Zhang(张正龙)

Citation: Chin. Phys. B, 2024, 33 (**3**): 033101. DOI: 10.1088/1674-1056/ad123d
Journal homepage: http://cpb.iphy.ac.cn; http://iopscience.iop.org/cpb

What follows is a list of articles you may be interested in

Polyhedral silver clusters as single molecule ammonia sensor based on charge transfer-induced plasmon enhancement

Jiu-Huan Chen(陈九环) and Xin-Lu Cheng(程新路)
Chin. Phys. B, 2023, 32 (**1**): 017302. DOI: 10.1088/1674-1056/ac6daf

Theoretical insights into photochemical ESITP process for novel DMP-HBT-py compound

Guang Yang(杨光)†, Kaifeng Chen(陈凯锋), Gang Wang(王岗), and Dapeng Yang(杨大鹏)
Chin. Phys. B, 2020, 29 (**10**): 103103. DOI: 10.1088/1674-1056/aba9bb

Exploration and elaboration of photo-induced proton transfer dynamical mechanism for novel 2-[1,3]dithian-2-yl-6-(7aH-indol-2-yl)-phenol sensor

Lei Xu(许磊), Tian-Jie Zhang(张天杰), Qiao-Li Zhang(张巧丽), Da-Peng Yang(杨大鹏)
Chin. Phys. B, 2020, 29 (**5**): 053102. DOI: 10.1088/1674-1056/ab8208

Ab initio investigation of excited state dual hydrogen bonding interactions and proton transfer mechanism for novel oxazoline compound

Yu-Sheng Wang(王玉生), Min Jia(贾敏), Qiao-Li Zhang(张巧丽), Xiao-Yan Song(宋晓燕), Da-Peng Yang(杨大鹏)
Chin. Phys. B, 2019, 28 (**10**): 103105. DOI: 10.1088/1674-1056/ab4042

Recent progress on photoluminescence from plasmonic nanostructures: Phenomenon, mechanism, and application

Tingting Yin(尹婷婷), Liyong Jiang(蒋立勇), Zexiang Shen(申泽骧)
Chin. Phys. B, 2018, 27 (**9**): 097803. DOI: 10.1088/1674-1056/27/9/097803

Microscopic mechanism of plasmon-mediated photocatalytic H_2 splitting on Ag–Au alloy chain

Yuhui Song(宋玉慧), Yirui Lu(芦一瑞), Axin Guo(郭阿鑫), Yifei Cao(曹逸飞), Jinping Li(李金萍), Zhengkun Fu(付正坤), Lei Yan(严蕾)†, and Zhenglong Zhang(张正龙)‡

School of Physics and Information Technology, Shaanxi Normal University, Xi'an 710119, *China*

(Received 2 November 2023; revised manuscript received 1 December 2023; accepted manuscript online 5 December 2023)

Alloy nanostructures supporting localized surface plasmon resonances has been widely used as efficient photocatalysts, but the microscopic mechanism of alloy compositions enhancing the catalytic efficiency is still unclear. By using time-dependent density functional theory (TDDFT), we analyze the real-time reaction processes of plasmon-mediated H_2 splitting on linear Ag–Au alloy chains when exposed to femtosecond laser pulses. It is found that H_2 splitting rate depends on the position and proportion of Au atoms in alloy chains, which indicates that specially designed Ag–Au alloy is more likely to induce the reaction than pure Ag chain. Especially, more electrons directly transfer from the alloy chain to the anti-bonding state of H_2, thereby accelerating the H_2 splitting reaction. These results establish a theoretical foundation for comprehending the microscopic mechanism of plasmon-induced chemical reaction on the alloy nanostructures.

Keywords: plasmon, photocatalysis, time-dependent density functional theory (TDDFT)

PACS: 31.15.ee, 36.40.Sx, 82.30.Hk **DOI:** 10.1088/1674-1056/ad123d

Plasmonic photocatalysis has made significant progress in converting solar energy into chemical energy, such as decomposition of molecules,[1] artificial photosynthesis,[2] and synthesis hydrocarbon fuels.[3] The microscopic mechanism of plasmon-induced photocatalysis has been attributed to local electromagnetic-field enhancement,[4] charge transfer,[5,6] and local thermal effects[7] generated by plasmon relaxation. Among them, transfer of hot carriers plays a crucial role in plasmon catalytic reactions.[8,9] Hot elctrons generated by plasmon decay can be transferred to reactant molecules through direct electron transfer or indirect electron transfer process.[10,11] In the direct electron transfer process, surface hybrid states can be formed because of strong interaction between the adsorbate and the metal, and plasmonic coupling with the surface hybrid states can generate hot electrons on the reactant directly.[12] In the indirect electron transfer process, the excited hot electrons interact with surrounding electrons and then transfer to the reactant molecules due to the electron tunneling effect.[8]

Alloy nanostructures with unique plasmonic property can significantly enhance the chemical reaction and is widely used in the plasmonic photocatalysis.[13] Ag–Au alloys have unique LSPR,[14] tunable optical properties,[15] and good chemical resistance,[16] usually better than pure metal nanostructures on photocatalysis.[17] Yue *et al.*[18] have found that the photocatalytic H_2-evolution rate has been increased with a factor of eight by transferring Ag nanoparticles into Ag–Au alloy nanoparticles due to the plasmon-induced stronger electromagnetic field. Li *et al.*[19] have discovered that Au@Ag nanoalloys exhibit about 1.6 times higher molecular decomposition efficiency compared to Au or Ag, and proposed the enhanced photocatalytic activity owing to more hot carriers on bimetallic nanoparticles by plasmon decay. In this sense, it is still disputed which kind of microscopic mechanisms is the most effective for alloy plasmon-enhanced reaction.

Here, we investigate the real-time dynamics of H_2 photosplitting on alloy Ag–Au chains irradiated by femtosecond laser pulses to reveal the atomic-scale reaction mechanism by TDDFT.[20,21] The splitting rate of H_2 is found to depend on the position and proportion of Au atoms in alloy chains, and specially designed Ag–Au alloy is more likely to induce H_2 photosplitting than pure Ag chain. Moreover the difference of H_2 photosplitting rate can be explained by comparing the occupation evolutions of the anti-bond states of H_2 adsorbed on different alloy chains. This research provides a deep understanding of the atomic-scale mechanism of plasmon-mediated photochemistry on the alloy nanostructures.

Electronic structures and dynamics coupled with the ionic motion are treated within the Ehrenfest scheme.[22] The electronic structures follow the time-dependent Kohn–Sham (TDKS) equations[23]

$$\mathrm{i}\hbar\frac{\partial}{\partial t}\varphi_i(\boldsymbol{r},t) = h_{\mathrm{ks}}(t)\varphi_i(\boldsymbol{r},t),$$

where the functions φ_i and h_{ks} are the KS orbitals and KS Hamiltonian, respectively. Table S1 presents the eigenvalue of KS orbitals for H_2 on Ag_5–Au. The ionic motion follows

†Corresponding author. E-mail: yanlei@snnu.edu.cn
‡Corresponding author. E-mail: zlzhang@snnu.edu.cn

© 2024 Chinese Physical Society and IOP Publishing Ltd

the classical Newtonian equations[24]

$$M_I\ddot{\boldsymbol{B}}_I = -\nabla_I\left[v(\boldsymbol{R}_I,t) - \int \frac{Z_I n(\boldsymbol{r},t)}{|\boldsymbol{R}_I-\boldsymbol{r}|}\,\mathrm{d}r + \sum_{J\neq I}\frac{Z_I Z_J}{|\boldsymbol{R}_I-\boldsymbol{R}_J|}\right],$$

where M_I, $\boldsymbol{R}_I$, and Z_I are the I-st nucleus mass, spatial location, and number of valence electrons, respectively. TDDFT can be effective in conjunction with LDA for dissociations[25] but it certainly has its limitations. Because the LDA holds that the exchange–correlation energy functional is only related to the value of the electron density at various points in space. During the process of dissociation, the change of electron density can result in the potential energy curve predicted by LDA deviating from the actual dissociation pathway. Moreover, the dissociation potential energy of LDA decreases exponentially as the relative coordinates approach infinity. Therefore, LDA is suitable for systems exhibiting a gradual change in charge density and systems with high charge density.[26]

We first compare the H_2 photosplitting on linear Ag_5–Au and Ag_6 atomic chains under an external laser pulse. In our time evolution simulation of the bond length, Ag and Au atoms are considered as mobile with initial interatomic distance of 2.89 Å, chosen from the experimental value for Ag chains on NiAl (110) surface.[27] The geometry configuration of H_2 adsorbed on the Ag_5–Au chain is shown in Fig. 1(a). Here, the laser pulse polarized in the z direction along the chain in Fig. 1(b) is modeled by a Gaussian wave packet expressed as

$$E(t) = E_{\max}\exp\left[-\frac{(t-t_0)^2}{2\tau^2}\right]\cos(\omega t-\omega t_0).$$

Here, the pulse width τ is 2.6 fs, and it reaches the maximum amplitude $E_{\max} = 1.5$ V/Å at the time $t = 9.8$ fs. Due to forbidding computational costs in TDDFT quantum dynamics simulations, we utilize a strong laser field to accelerate photoreactions to make the simulations of H_2 photosplitting feasible. The laser frequency is chosen as $\hbar\omega = 1.54$ eV, which is the plasmonic energy of Ag_5–Au chain obtained from the optical absorption spectrum in Fig. S1. The laser fluence we applied is 0.08 J/cm^2, which is widely available and easily applied in typical ultrafast laser experiments.[28] In addition, laser pulse duration is too short ($\sim$ 10 fs) to induce significant local heating or structural damage in the Ag–Au clusters. The kinetic energy of each silver and gold atom is increasing with the time and the value is in the range of 0.1–1.3 eV at the end of simulation time of $t = 20$ fs with $E_{\max} = 1.5$ V/Å (Fig. S2(a)). The bondlength of Ag_5–Au decreases form 2.89 Å at $t = 0$ fs to 2.85 Å at $t = 20$ fs and that of Ag_1–Ag_2 increases from 2.89 Å to 2.98 Å (Fig. S2(b)). We estimate the cluster would be destroyed when the simulation is continued beyond 100 fs. In addition, the plasmon mode in Fig. S3 shows that the entire charge distribution remains in dipole mode.

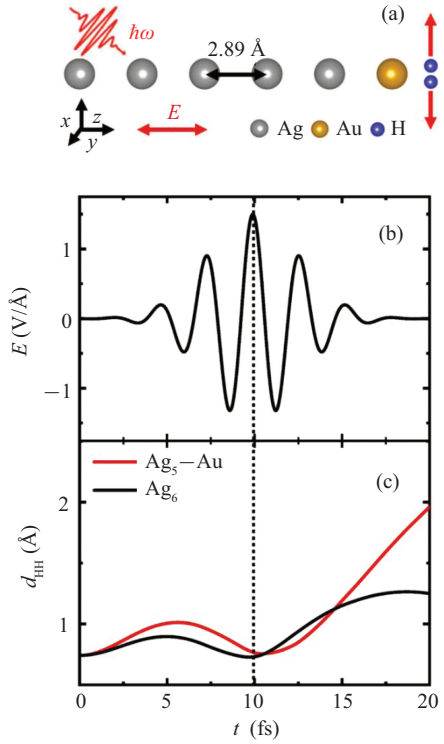


Fig. 1. (a) Schematic showing plasmon-induced H_2 splitting on Ag_5–Au atomic chain under the laser field polarized in the z direction. (b) Time-dependent electric field of the laser pulse. The maximum amplitude $E_{\max} = 1.5$ V/Å and laser frequency is 1.54 eV. Under this laser, time evolution of bond length d_{HH} on the Ag_5–Au and Ag_6 chains (c). The vertical dotted line denotes the time at which laser field reaches its maximum strength.

To investigate the photo-induced dynamics response, we calculate the time-dependent H–H bond length d_{HH} under the same laser field on Ag_5–Au and Ag_6 chains in Fig. 1(c). For the sake of simplicity in the following, we will consider the H_2 molecule split if the bond length d_{HH} is greater than 1.5 Å. On the Ag_5–Au chain, the period of H_2 oscillation is 10.4 fs, and the bond length keeps increasing from $d_{HH} = 0.7$ Å at $t = 10.5$ fs to $d_{HH} = 1.9$ Å at $t = 20$ fs, indicating that the H–H bond breaks on the Ag_5–Au chain. Under the same condition, no dissociation is observed up to $t = 20$ fs on the Ag_6 chain, despite that H_2 is distorted with oscillating period of 9.5 fs and the maximum bond length reaches 1.2 Å. The result suggests that H_2 photosplitting on Ag_5–Au alloy chain is easier than that on pure Ag_6 chain.

In order to uncover the underlying mechanism of higher catalytic efficiency of Ag_5–Au alloy chain, we compare and analyze time-evolved occupation of anti-bonding (AB) states of H_2 for the two complexes, fixing all atoms at initial positions under the same laser field in Fig. 2(a). AB states of H_2 on Ag_5–Au considered here are LUMO (lowest unoccupied molecular orbital) + 3 and LUMO + 5, where hydrogen contributes the most to the states (Fig. 2(c)). The occupation of AB states is calculated by projecting the time-dependent wavefunction onto the ground state of AB states.[29] The atomic coordinates of ground state are chosen as the geometry at the

time $t = 0$ fs and not same as snapshot of the Ehrenfest dynamics. It can be identified that the occupation amount of AB states of H_2 on the Ag_5–Au chain is greater than that on the Ag_6 chain, implying that the introduction of the Au atom increases the transition possibility of electron to the AB state of H_2. Thus, H_2 photosplitting on Ag_5–Au alloy chain is easier than that on pure Ag_6 chain because more hot electrons transfer to the AB states of H_2.

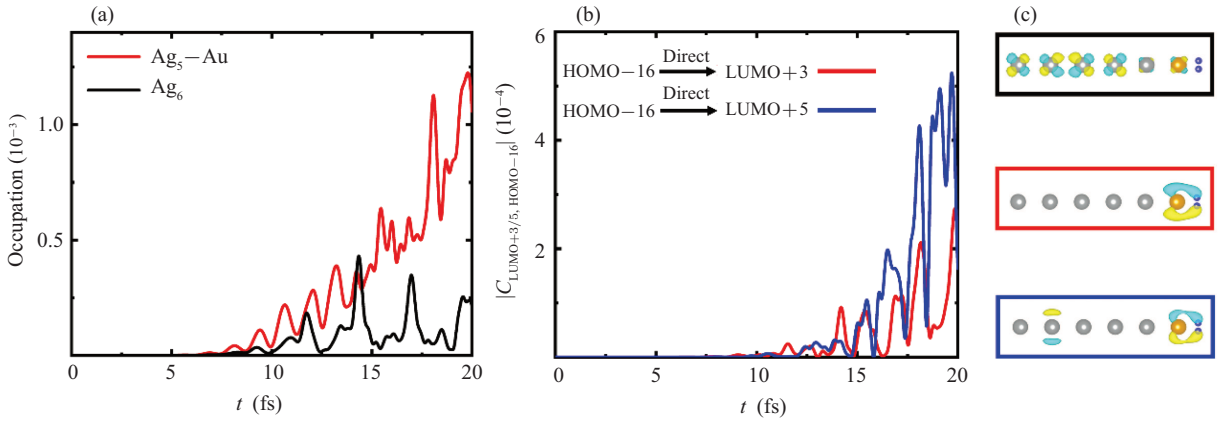


Fig. 2. (a) Time-dependent occupation of AB states on the Ag_5–Au and Ag_6 chains with a field strength of 0.05 V/Å. (b) Time-evolved transition coefficient $|C_{\mathrm{LUMO+3/5,\,HOMO-16}}|^2$ from the occupied state HOMO − 16 to AB states LUMO + 3 and LUMO + 5 of H_2 on the Ag_5–Au chain. (c) The wavefunctions of HOMO − 16 (black), LUMO + 3 (red), and LUMO + 5 (blue) shown in boxes. Here, the isosurface value of wavefunctions is 0.1 $Å^{-3}$. HOMO: highest occupied molecular orbital, LUMO: lowest unoccupied molecular orbital.

To describe the ultrafast carrier dynamics of plasmon-induced H_2 photosplitting on Ag_5–Au alloy chain, we calculate the time-dependent transition coefficients from the occupied state (HOMO − 16) showing the largest transition to AB states of H_2 (LUMO + 3 and LUMO + 5) in Fig. 2(b). The wavefunctions of HOMO - 16 mainly distributes on d-orbital of alloy atom and that of LUMO + 3 and LUMO + 5 correspond to the AB states of hydrogen molecule (Fig. 2(c)), indicating that electrons transfer from alloy chain to hydrogen molecule is direct charge transfer mechanism.[30] Furthermore, the other occupied orbitals contributing to LUMO + 3 and LUMO + 5 also have d-electron character (Fig. S4). These transition coefficients in Fig S4 display a gradual increase in amplitude, corresponding to hot electron generation by plasmon decay.[31] It can be concluded that plasmon-induced hydrogen splitting on Ag_5–Au chain is owing to the direct electrons transfer from d-electron of alloy chain to the AB state of H_2. Li *et al.*[19] have discovered that plasmonic Au@Ag nanoalloys in experiments exhibit about 1.6 times higher molecular decomposition efficiency compared to Au or Ag under visible light irradiation. Wu *et al.*[32] has confirmed experimentally direct charge transfer from the Au tip to CdSe nanorod with quantum efficiencies exceeding 24%. The experimental results are consistent with our theoretical results that the photocatalytic ability of Ag_5–Au alloys to decompose hydrogen is 1.57 times higher than that of pure silver chains, owing to more electrons directly transfer from alloy chain to H_2.

The splitting rates of H_2 absorbed on the Ag–Au alloy chain are also affected by the position of Au atom. The six configurations of H_2 absorbed on the different alloy chains are depicted in Fig. 3(a). To investigate the photo-induced response, the time-dependent H–H bond length d_{HH} is calculated for the six systems under the same field strength in Fig. 3(b). At the end of the simulation time $t = 20$ fs, d_{HH} is 1.96 Å, 1.4 Å, 1.23 Å, 0.98 Å, 0.93 Å, and 0.93 Å and decreases in turn for Ag_5–Au, Ag_4–Au–Ag, Ag_3–Au–Ag_2, Ag_2–Au–Ag_3, Ag–Au–Ag_4, and Au–Ag_5, respectively. The ability of plasmons to induce hydrogen decomposition increases with Au atom approaching H_2 from the general trend. Obviously, when Au atom on the Ag–Au chain approaching H_2, the rate of H_2 photosplitting increases.

To understand the influence of Au atom position in Ag–Au chains on H_2 splitting rate, time-evolved occupation of AB states of H_2 for the six complexes under the same field strength is analyzed. The occupation comparison of typical complexes of H_2 absorbed on Ag_5–Au and Au–Ag_5 is shown in Fig. 3(c). We can identify that the occupation amount of AB state of H_2 on Ag_5–Au chain is greater than that on the Au–Ag_5 chain, resulting in the increased reaction rate on Ag_5–Au chain. The occupation comparison of the other four complexes in Fig. S5 is also consistent with the H_2 reaction rate in Fig. 3(b). The electronic structure of alloy chain could be influenced by substrate NiAl (110). Resonant energy of surface plasmon maybe shift with the substrate considered. The model of isolated Na atomic chain and Ag chain has been used for study of plasmon resonances.[33,34] The field enhancements (FE) at the position of H_2 in the different atom chains and the corresponding H–H bond length d_{HH} at $t = 20$ fs have been calculated (Fig. S6). The trend of FE is different with that of the d_{HH}, indicating that FE is not the prominent drivers for the reaction. The results show that more electrons transfer from alloy chain to the AB state of H_2 with Au atom approaching H_2, further enhancing the reaction.

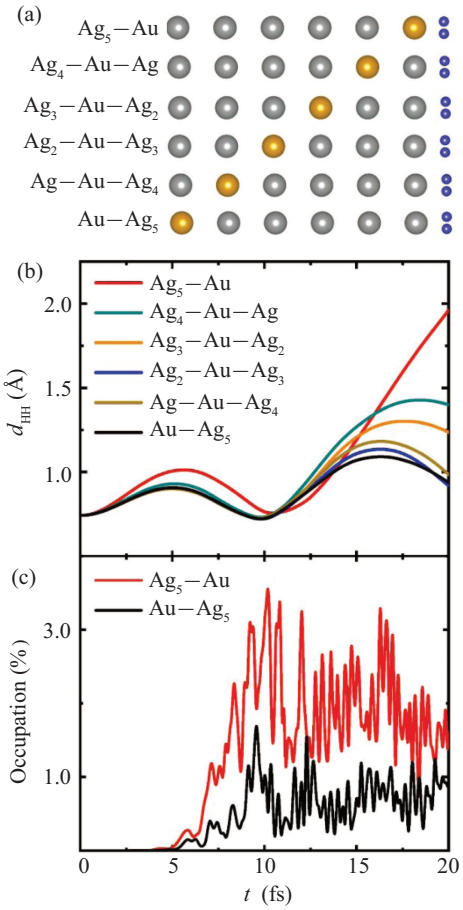


Fig. 3. (a) Schematic showing H_2 absorbed on Ag_5–Au, Ag_4–Au–Ag, Ag_3–Au–Ag_2, Ag_2–Au–Ag_3, Ag–Au–Ag_4, and Au–Ag_5 alloy chains. (b) Time evolution of bond length d_{HH} under laser illumination with a maximum field strength $E_{max} = 1.5$ V/Å for the six systems. Under the same laser, time-dependent occupation of AB state of H_2 on Ag_5–Au and Au–Ag_5 chains (c).

The effect of the proportion of Au atoms in Ag–Au alloy chains on plasmon-driven reaction is further explored. The three geometric configurations of H_2 absorbed on Ag_3–Au_3, Ag_4–Au_2, and Au_5–Ag alloy chains are depicted in Fig. 4(a). To investigate the photoinduced response, the time-dependent H–H bond length d_{HH} is calculated for the three systems under the same field strength in Fig. 4(b). At the end of the simulation time $t = 20$ fs, d_{HH} is 3 Å, 2.3 Å, and 2.1 Å for Ag_3–Au_3, Ag_4–Au_2, for Au_5–Ag, respectively. The H_2 splitting rate increases with the increased proportion of Au atoms in the Ag–Au alloy chains. In order to explain such phenomenon, time-evolved occupations of AB state of H_2 for the three complexes under the same field strength are analyzed in Fig. 4(c). The oscillation trend of the occupations of AB states is very similar during the whole reaction process for the three complexes. The occupation amount of AB state of H_2 increases slightly with the increased proportion of Au atoms leading to the enhanced reaction trend in Fig. 4(b) The results show that more electrons transfer from the alloy chain to the AB state of H_2 with increased proportion of Au atoms in the Ag–Au alloy chains, resulting in the elevated reaction rate.

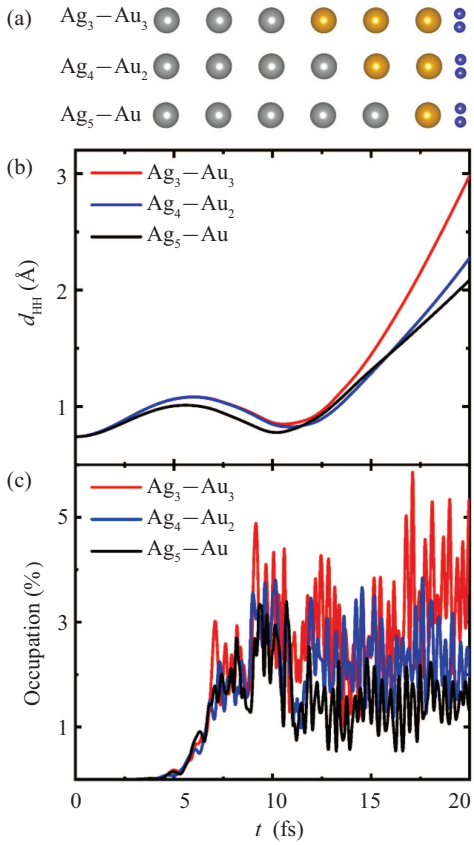


Fig. 4. (a) Schematic showing H_2 absorbed on Ag_3–Au_3, Ag_4–Au_2, and Ag_5–Au atomic chains. (b) Time evolution of bond length d_{HH} under laser illumination with a maximum field strength $E_{max} = 1.8$ V/Å for the three alloy chains. (c) Time-dependent occupation of AB states of H_2 for the three complexes.

In conclusion, the plasmon-mediated H_2 splitting dynamics on the Ag–Au alloy chains using TDDFT is investigated. We demonstrate that the ability of plasmons to induce H_2 decomposition increases with Au atom approaching H_2, and the increased proportion of Au atoms in the Ag–Au chains, which indicates that specially designed Ag–Au alloy is more likely to induce H_2 splitting than pure Ag chain. Especially, we find direct electrons transfer from the atomic chain to the AB state of H_2 by plasmon decay, driving the reaction. The results provide insights towards a complete fundamental understanding of plasmon-induced chemical reactions on the alloy nanoparticles at the microscopic scale and may help to improve the energy conversion efficiency in plasmon-assisted photochemistry. It is of great significance to explore the multi-scale effects of plasmon-induced chemical reaction from atomic scale to macroscopic scale. Due to substantial computational requirements of TDDFT method, calculating macroscopic cluster systems far exceeds our current computational capacity. In future work, we will extend this study to nanoscale levels such as Ag_{55} and Ag_{147}.

Acknowledgements

Project supported by the National Key Research and Development Program of China (Grant Nos. 2020YFA0211300

and 2021YFA1201500), the National Natural Science Foundation of China (Grant Nos. U22A6005, 92150110, 12074237, and 12304426), the Natural Science Foundation of Shaanxi Province, China (Grant No. 2024JC-JCQN-07), the Fundamental Science Foundation of Shaanxi Province, China (Grant No. 22JSZ010), and the Fundamental Research Funds for Central Universities (Grant Nos. GK202201012 and GK202308001).

References

[1] Yan L, Ding Z, Song P, Wang F and Meng S 2015 *Appl. Phys. Lett.* **107** 083102
[2] Valenti M, Venugopal A, Tordera D, Jonsson M P, Biskos G, Schmidt-Ott A and Smith W A 2017 *ACS Photon.* **4** 1146
[3] Hu C, Chen X, Low J, Yang Y W, Li H, Wu D, Chen S, Jin J, Li H, Ju H, Wang C H, Lu Z, Long R, Song L and Xiong Y 2023 *Nat. Commun.* **14** 221
[4] Wu S, Chen Y and Gao S 2022 *Phys. Rev. Lett.* **129** 086801
[5] Zhai L, Gebre S T, Chen B, Xu D, Chen J, Li Z, Liu Y, Yang H, Ling C, Ge Y, Zhai W, Chen C, Ma L, Zhang Q, Li X, Yan Y, Huang X, Li L, Guan Z, Tao C L, Huang Z, Wang H, Liang J, Zhu Y, Lee C S, Wang P, Zhang C, Gu L, Du Y, Lian T, Zhang H and Wu X J 2023 *Nat. Commun.* **14** 2538
[6] Zhang Y, Nelson T, Tretiak S, Guo H and Schatz G C 2018 *ACS Nano* **12** 8415
[7] Kong T, Zhang C, Lu J, Kang B, Fu Z, Li J, Yan L, Zhang Z, Zheng H and Xu H 2021 *Nanoscale* **13** 4585
[8] Zhang Y, He S, Guo W, Hu Y, Huang J, Mulcahy J R and Wei W D 2018 *Chem. Rev.* **118** 2927
[9] Chu W, Tan S, Zheng Q, Fang W, Feng Y, Prezhdo O V, Wang B, Li X Z and Zhao J 2022 *Sci. Adv.* **8** eabo2675
[10] Kumar P V, Rossi T P, Marti-Dafcik D, Reichmuth D, Kuisma M, Erhart P, Puska M J and Norris D J 2019 *ACS Nano* **13** 3188
[11] Wang S, Huang M, Wu Y N, Chu W, Zhao J, Walsh A, Gong X G, Wei S H and Chen S 2022 *Nat. Comput. Sci.* **2** 486
[12] Foerster B, Joplin A, Kaefer K, Celiksoy S, Link S and Sonnichsen C 2017 *ACS Nano* **11** 2886
[13] Gilroy K D, Ruditskiy A, Peng H C, Qin D and Xia Y 2016 *Chem. Rev.* **116** 10414
[14] Mayer K M and Hafner J H 2011 *Chem. Rev.* **111** 3828
[15] Johnson H M, Dasher A M, Monahan M, Seifert S and Moreau L M 2022 *Nanoscale* **14** 4519
[16] Babu R S, Colenso H R, Gouws G J, AuguiB and Moore C P 2023 *IEEE Sens. J.* **23** 10420
[17] Kamimura S, Yamashita S, Abe S, Tsubota T and Ohno T 2017 *Appl. Catal. B* **211** 11
[18] Yue X, Hou J, Zhao H, Wu P, Guo Y, Shi Q, Chen L, Peng S, Liu Z and Cao G 2020 *J. Energy Chem.* **49** 1
[19] Li S, Zhao J, Liu G, Xu L, Tian Y, Jiao A and Chen M 2021 *Nanotechnology* **32** 125401
[20] Ramakrishna K, Cangi A, Dornheim T, Baczewski A and Vorberger J 2021 *Phys. Rev. B* **103** 125118
[21] Weissker H C and Mottet C 2011 *Phys. Rev. B* **84** 165443
[22] Tavernelli I, Röhrig U F and Rothlisberger U 2005 *Mol. Phys.* **103** 963
[23] Runge E and Gross E K U 1984 *Phys. Rev. Lett.* **52** 997
[24] Theilhaber J 1992 *Phys. Rev. B* **46** 12990
[25] Castro A 2013 *Chem. Phys. Chem.* **14** 1488
[26] Yabana K and Bertsch G F 1996 *Phys. Rev. B* **54** 4484
[27] Nazin G V, Qiu X H and Ho W 2003 *Phys. Rev. Lett.* **90** 216110
[28] Michel P, Benz W and Richardson D C 2003 *Nature* **421** 608
[29] Yan L, Wang F and Meng S 2016 *ACS Nano* **10** 5452
[30] Zhang Y, Yan L, Guan M, Chen D, Xu Z, Guo H, Hu S, Zhang S, Liu X, Guo Z, Li S and Meng S 2022 *Adv. Sci.* **9** 2102978
[31] Yan L, Xu J, Wang F and Meng S 2018 *J. Phys. Chem. Lett.* **9** 63
[32] Wu K, Chen J, McBride J R and Lian T 2015 *Science* **349** 632
[33] Yan J, Yuan Z and Gao S W 2007 *Phys. Rev. Lett.* **98** 216602
[34] Yan J and Gao S 2008 *Phys. Rev. B* **78** 235413